

Giant landslide triggerings and paleoprecipitations in the Central Western Andes: The aricota rockslide dam (South Peru)



Fabrizio Delgado^{a,b,c}, Swann Zerathe^{b,*}, Laurence Audin^b, Stéphane Schwartz^b, Carlos Benavente^c, Julien Carcaillet^b, Didier L. Bourlès^d, Aster Team^{d,1}

^a Especialidad Ingeniería Geológica, Facultad de Ciencias e Ingeniería. Pontificia Universidad Católica del Perú, Av. Universitaria 1801, San Miguel, Lima 15088, Perú

^b Univ. Grenoble Alpes, Univ. Savoie Mont Blanc, CNRS, IRD, IFSTTAR, ISTERRE, 38000 Grenoble, France

^c Instituto Geológico, Minero y Metalúrgico INGEMMET, Av. Canadá 1470, Lima, Perú

^d Aix-Marseille Univ., CNRS, IRD, Coll. France, UM 34 CEREGE, Technopôle de l'Environnement Arbois-Méditerranée, BP80, 13545 Aix-en-Provence, France

ARTICLE INFO

Article history:

Received 5 February 2019

Received in revised form 15 October 2019

Accepted 30 October 2019

Available online 2 November 2019

Keywords:

Giant landslide dam

Central Western Andes

¹⁰Be dating

Triggering factors

ABSTRACT

The central part of the Western Andes holds an exceptional concentration of giant paleolandslides involving very large volumes of rock material ($v > \text{km}^3$). While those gravitational slope failures are interpreted consensually as an erosional response to the geodynamic activity of the Andes (relief formation and tectonic activity), the question of their triggering mechanisms remains enigmatic. To clarify the respective roles of climatic versus seismic forcing on the Andean landslides, new temporal constraints on paleo movements are essential. Here, we focus on one of those giant slope failures, the Aricota giant rockslide that damned the Locumba valley in southern Peru. We conducted fieldwork, high-resolution DEM analysis and cosmogenic nuclide dating to decipher its development history and failure mechanisms. Our results point to the occurrence of two successive events. A giant failure mobilizing a rock volume of ca. 2 km^3 first produced a dam at $17.9 \pm 0.7 \text{ ka}$. Considering its height of ca. 600 m, the Aricota rockslide dam is one of the three largest landslide dams worldwide. At $12.1 \pm 0.2 \text{ ka}$, a second event produced ca. 0.2 km^3 of material, and the rock-avalanche debris spread out over the dam. As the chronology of those two events is pointing to the two main paleoclimatic pluvial periods in this region (Heinrich Stadial 1a and Younger Dryas), we favor the interpretation of a climatic forcing. At a regional scale, the concomitant aggradation of alluvial terraces and fan systems along the nearby valleys highlights higher regional erosion, sediments supply and mass-wasting events during those paleoprecipitation events and strengthens this conclusion.

© 2019 Elsevier B.V. All rights reserved.

1. Introduction

The Western flank of the Central Andes (south Peru - north Chile) holds one of the most exceptional concentrations of giant landslides worldwide (Crosta et al., 2014). Those gravitational instabilities mobilize large volume of rock material ($> 10^9 \text{ m}^3$), with debris propagation over long distance ($> 10^3 \text{ m}$) affecting the Western Cordillera from elevations between 4500 m to sea level (e.g. Wörner et al., 2002; Strasser and Schlunegger, 2005; Pinto et al., 2008; Crosta et al., 2014). This Andean area is particularly active geodynamically, related to the long-term convergence between the Nazca and the South America plates. The global shortening is associated

with the relief construction, producing instantaneous deformation (crustal seismicity) coupled with long-term processes of surface uplift and volcanism (Thouret et al., 2017; Benavente et al., 2017). In this region, the large-scale landsliding is suspected to be an efficient relief erosion mechanism at regional scale (Mather et al., 2014).

Additionally, the Western Andean flank presents a climatic setting marked by a dominant hyper-aridity persisting at least since 20 million years (e.g. Dunai et al., 2005). This particular climate environment, with very low denudation rates (typically $1\text{--}10 \text{ mm.kyr}^{-1}$; Nishiizumi et al., 2005; Madella et al., 2018), allows the local preservation of landscape over hundreds of thousands years (e.g. Zerathe et al., 2017). This offers a unique opportunity to track gravitational slope processes over a temporal scale currently unknown, close to the timing of the orogen evolution (Hermanns et al., 2001).

* Corresponding author.

E-mail address: swann.zerathe@ird.fr (S. Zerathe).

¹ Georges Aumaître and Karim Keddadouche.

On the other hand, the development of such giant landslides in a desert environment raise the question of their triggering conditions and failure mechanisms. In the literature, this question is largely debated with two main opposite views implying seismicity versus climatic controls (Moreiras and Sepúlveda, 2015). For examples, McPhillips et al. (2014) suggest that at a millennial-scale, the record of landslides activity in the Andes is mainly consistent with earthquake trigger, whereas Margirier et al. (2015) identified a correlation between the activity phases of a giant paleolandslide (Chuquibamba, south Peru) and wet climatic events on the Altiplano. As pointed by Moreiras and Sepúlveda (2015), in order to push away the limit of this debate and to decipher the respective role of each forcing, new temporal constraints on giant Andean paleolandslides are required. Indeed, while numerous giant landslides have been identified along the western Andean flank (Audin and Bechir, 2006; Crosta et al., 2014), the great majority of them have not been dated yet. In this context, the cosmogenic nuclide dating, applied to either landslide scarps or boulders, is specifically pertinent to constrain the timing of slope evolution (Zerathe et al., 2017; Crosta et al., 2017).

In this paper, we combined geomorphological analysis based on high resolution Pléiades DEMs and geochronological dating using ^{10}Be produced within quartz minerals (in situ-produced ^{10}Be) in order to document the chronology and to determine the context in which the Aricota giant rockslide dam (Central Western Andes, South Peru) occurred.

2. Geological context and landslide setting

The study area is located in the South Peru at $\sim 17^\circ\text{S}$ latitude, along the Western flank of the Central Andean Cordillera (Fig. 1), where ongoing subduction of the Nazca Plate occurs with a convergence velocity of about 62 mm.yr^{-1} (e.g. Villegas-Lanza et al., 2016). The geomorphology of this region is contrasted and shows from West to East: (1) a coastal cordillera with a maximum elevation of 1000 m a.s.l., (2) the Western Cordillera with elevations comprised between 1000 and 4500 m a.s.l., and (3) the Altiplano plateau reaching 5000 m a.s.l. This western flank of the Andes is carved by deep valleys and canyons related to a regional uplift (e.g. Thouret et al., 2007; Schildgen et al., 2009; Gunnell et al., 2010 and references therein). The Western Cordillera is affected by westward major thrusts (Fig. 1) oriented parallel to the subduction trench (Hall et al., 2012; Benavente et al., 2017). The timing and the processes involved in the creation of the Andean relief in this region are still debated. Sempere et al. (2008) propose a rapid uplift of about 2.5 km since the Late Miocene (11 to 6 Ma) in response to a large-scale mantle delamination. Armijo et al. (2015) propose that the topography was controlled by crustal thickening during the Paleogene (50 to 30 Ma) in response to the tectonic shortening of the Central Andes. This process is responsible for aridity increase of the Atacama Desert during the Neogene (Evenstar et al., 2015). Recently, Thouret et al. (2017) provide a compilation of $^{40}\text{Ar}/^{39}\text{Ar}$ and U/Pb dating of ignimbrite deposit covering this region, which helped to decipher the canyon incision chronology. Their dataset suggest that uplift was gradual over the past 25 Ma and accelerated after 9 Ma. The valley incisions start around 11–9 Ma and accelerate between 5 and 4 Ma. Pleistocene uplift rates of 0.2 to 0.4 mm.yr^{-1} have been derived from cosmogenic dating (Hall et al., 2012), and interpreted as a combination of tectonic shortening along steep westvergent faults of the western flank and isostatic responses to fluvial erosion associated with large scale landslide processes. The same conclusion is reached by Viveen and Schlunegger (2018) showing uplift at the Quaternary time scale in the Moquegua region. However, at the scale of the Peruvian forearc, their conclusions open other perspectives showing possible alter-

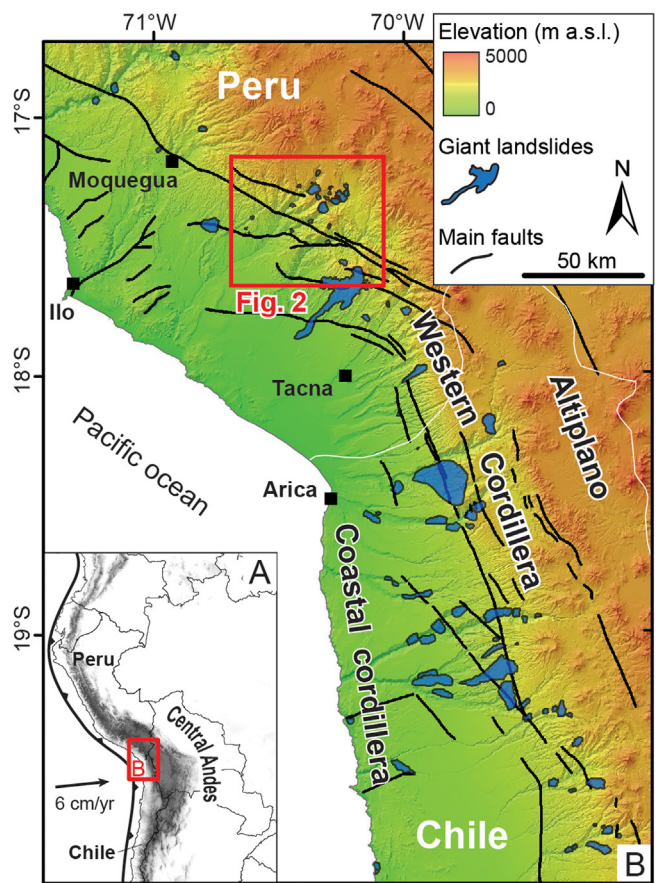


Fig. 1. Morpho-tectonic context of the Central Western Andes and location of the study area. Hillshade and elevation are produced using the ASTER DEM (resolution 30 m). Main faults are reported from Hall et al. (2012); Armijo et al. (2015) and Benavente et al. (2017). The database of giant landslides is compiled from Audin and Bechir (2006); Crosta et al. (2014); Mather et al. (2014); Zerathe et al. (2017) and adding personal mapping from this study.

nating phases of compressional and transtensional tectonics during the Cenozoic.

The progressive Cenozoic onset of the Andean relief acted as an important topographic barrier impeding the cross of cloud currents and precipitation from the Amazonian basin (Houston and Hartley, 2003). As a result, hyper-arid conditions have developed and still currently prevail in the so-called Atacama Desert, along the Western Central Andes, allowing for long-term preservation of landscapes (up to several millions of years, e.g. Dunai et al., 2005). As contrasting with this long-term dry climate, the flank of Western Central Andes, between latitudes 17°S and 20°S , holds an exceptional concentration of some of the largest landslides identified at the Earth surface (Fig. 1). The imprint of those giant landslides have been progressively identified and mapped since a decade (e.g. Audin and Bechir, 2006; Crosta et al., 2014). From North to South, some impressive examples among others are: the Chuquibamba landslide - 40 km^3 (Margirier et al., 2015; Thouret et al., 2017), the Caquilluco landslide - 15 km^3 (Zerathe et al., 2017), the Lluta landslide - 26 km^3 (Wörner et al., 2002; Strasser and Schlunegger, 2005), the Minimini landslide - $v>5 \text{ km}^3$, the Latagualla landslide - 5.4 km^3 (Pinto et al., 2008) or the Magnifico landslide - 0.2 km^3 (Mather et al., 2014; Crosta et al., 2017). Only few of those giant landslides have been precisely dated (e.g. Zerathe et al., 2017; Crosta et al., 2017). Paleo-climatic variations and/or active tectonic and seismicity are considered both as possible factors of forcing. However, mainly because of the lack precise of chronological constraints on

these events, there is no consensus to date about the reason of their triggerings (McPhillips et al., 2014; Margirier et al., 2015).

In this paper, we focus on one of those giant landslides, the Aricota rockslide dam. It developed in the middle of the Locumba valley whose basin extends across the whole Western Cordillera, from the Altiplano down to Pacific Ocean. The Aricota rockslide generated a large dam in the Locumba valley, forming a 6 km-long lake. The lithology observed around the valley is dominated by volcano-sedimentary rocks (Fig. 2). The Aricota rockslide affects geological series that are almost horizontal. From the valley bottom to the plateau, we observe the following stratigraphic cross section: Cretaceous andesite and rhyolite of the Quellaveco formation, Paleogene silt and shales of the Tarata formation and Neogeneous ignimbrite of the Huayllillas formation unconformably covering the former (Fig. 2). The Cretaceous layers are cut by intrusive granite at the north-east of the Aricota rockslide zone. Neotectonic faults activities have been described recently south-west of the Aricota rockslide, mainly along the Incapuquio fault system and the Purgatorio fault (Hall et al., 2012; Benavente et al., 2017). The Incapuquio fault system is a sub-vertical lineament of ~400 km in length with a northwest-southeast trending direction and accommodates left lateral transpressive displacement. The Purgatorio fault accommodates right lateral transpressive displacement which has produced at least two ruptures during the last thousands years with superficial offsets of several meters (Benavente et al., 2017).

On the Aricota rockslide dam site, two hydroelectric plants, Áricota I and II (35 MW) were built in 1967. The continuous pumping of water caused a drop of the lake level of ~100 m in the last 50 years, which allow studying paleo shorelines revealed by diatomite deposits (Placzek et al., 2001). Placzek et al. (2001) obtained radio-carbon calibrated ages ranging between ca. 300 and 7000 yr B.P., pointing to high lake levels around 6100 yr B.P. and 1700–1300 yr B.P. and giving a minimum age of ca. 7 ka for the rockslide-dam emplacement. They identified in the morphology the existence of two successive failure events. However, the precise chronology of this rockslide, the failure and triggering mechanisms remain unknown yet.

3. Methods

3.1. Pléiades DEM elaboration and mapping

To identify and map the structures and deposits associated to the Aricota giant rockslide activity, we combine geomorphic and tectonic observations based on field data, analyses of high-resolution Digital Elevation Model (DEM) and Google Earth images. A high-resolution DEM was derived from two stereo images acquired by the Pléiades satellites on October 2015. The full resolution of these optical images is 0.7 m and their orientation was assessed using the Rational Polynomial Coefficient (RPC) provided in their ancillary data. We generated the DEM using the open source software Ames Stereo Pipeline (ASP) developed by NASA (Broxton and Edwards, 2008) and followed the three-step procedure. First, each image was map-projected using the low-resolution (30 m) SRTM DEM. Then the two images were bundle-adjusted based on automatically extracted tie points, before finding the disparities. The third step involved finding the intersection of all the rays coming from the homologous points of the image pair. This step leads to a point cloud of the surface topography, which is then converted onto a 2-m resolution grid (Fig. 3A). Field campaigns were conducted in 2014 and 2015 to (1) validate the observations/interpretations made about the different deposits and related events within the rockslide mass, and (2) to sample boulders and scarps for cosmogenic nuclide surface exposure dating.

3.2. Cosmogenic nuclide surface exposure dating

In order to determine the ages of the different events that occurred on the Aricota rockslide area, a sampling strategy was designed according to our geomorphological mapping. Seventeen samples were selected (Fig. 3B). In order to constrain an accurate long-term and local denudation rate, one sample (AR1) was taken on the eroding surface (presumed at steady state) that is located on the plateau above the rockslide scarp at ca. 3700 m a.s.l.. Three samples (AR3, AR4 and AR5) were extracted from the free-face of two preserved sub vertical scarps (bedrock). Thirteen samples were extracted from boulders distributed all over the rockslide mass, including six samples (AR14 to AR21) from the main dam and seven others (AR6 to AR12, and AR27 to AR29) from a rock-avalanche deposit located on top of the dam (Fig. 3B). A last boulder, AR29, has been taken tentatively to estimate past variations of the Aricota lake level (Fig. 3B). Indeed, despite belonging morphologically to the rock-avalanche deposit, this boulder stands at an elevation that is of about 40 m below the pre-1967 lake level (date of artificial lake lowering by pumping). In other words, before 1967, tens of meters of water, sufficient to protect quasi-completely the AR29 boulder from cosmic ray primary and secondary particles, were covering it. Thus, any concentration measured in this sample might represent periods of past lake level drop that would be large enough to allow exposing the AR29 boulder to cosmic ray particles (at ten meters depth, the cosmogenic nuclide production rates are less than 0.2% that at the surface, Gosse and Phillips, 2001).

In general, we paid special attention to select boulders whose height and length were higher than 2 m and with no trace of post-deposition toppling, nor large desquamations. Elevation, latitude and longitude were recorded with a handle GPS. Pictures of the boulders are provided in the supplementary material.

Sample preparation and ^{10}Be chemical extraction were achieved following routine procedure, which is detailed in the supplementary information, at the GTC Plateform, ISTerre laboratory (Grenoble, France). $^{10}\text{Be}/^{9}\text{Be}$ measurements were performed at the French AMS National Facility, located at CEREGE in Aix-en-Provence (Arnold et al., 2013). $^{10}\text{Be}/^{9}\text{Be}$ ratios were calibrated against the in-house standard STD-11, using an assigned $^{10}\text{Be}/^{9}\text{Be}$ ratio of $(1.191 \pm 0.013) \times 10^{-11}$ (Braucher et al., 2015). Uncertainties on ^{10}Be concentrations (reported as 1σ) are calculated according to the standard error propagation method using the quadratic sum of the relative errors and include a conservative 0.5% external machine uncertainty (Arnold et al., 2010), a 1.08% uncertainty on the certified standard ratio, a 1σ uncertainty associated to the mean of the standard ratio measurements during the measurement cycles, a 1σ statistical error on counted events and the uncertainty associated with the chemical and analytical blank correction.

Denudation rates and exposure durations were both calculated using the MATLAB®-based CRONUScalc program, developed by Marrero et al. (2016). We applied a globally calibrated ^{10}Be spallation production rate of $4.09 \pm 0.35 \text{ at.gr}^{-1}.\text{yr}^{-1}$ (sea level and high latitude; Borchers et al., 2016) which was scaled at the geographical and altitudinal location of each sampling site using the LSD scaling scheme (SF; Lifton et al., 2014; see details in the supplementary information).

We initially calculated long-term denudation rates for this area. As this will be detailed in the following results, in addition to the dedicated sample AR1, two other samples (AR14 and AR15) were considered for denudation rates calculation.

Finally, exposure duration calculations were performed considering this locally constrained denudation rate. Both analytical and total uncertainties (1σ) are reported. Analytical age uncertainties (i.e. internal) include uncertainties of the measured ^{10}Be concentrations (Table 1, supplementary data), pressure ($\pm 5 \text{ hPa}$), sample thickness ($\pm 1 \text{ cm}$), shielding factor (± 0.01), denudation

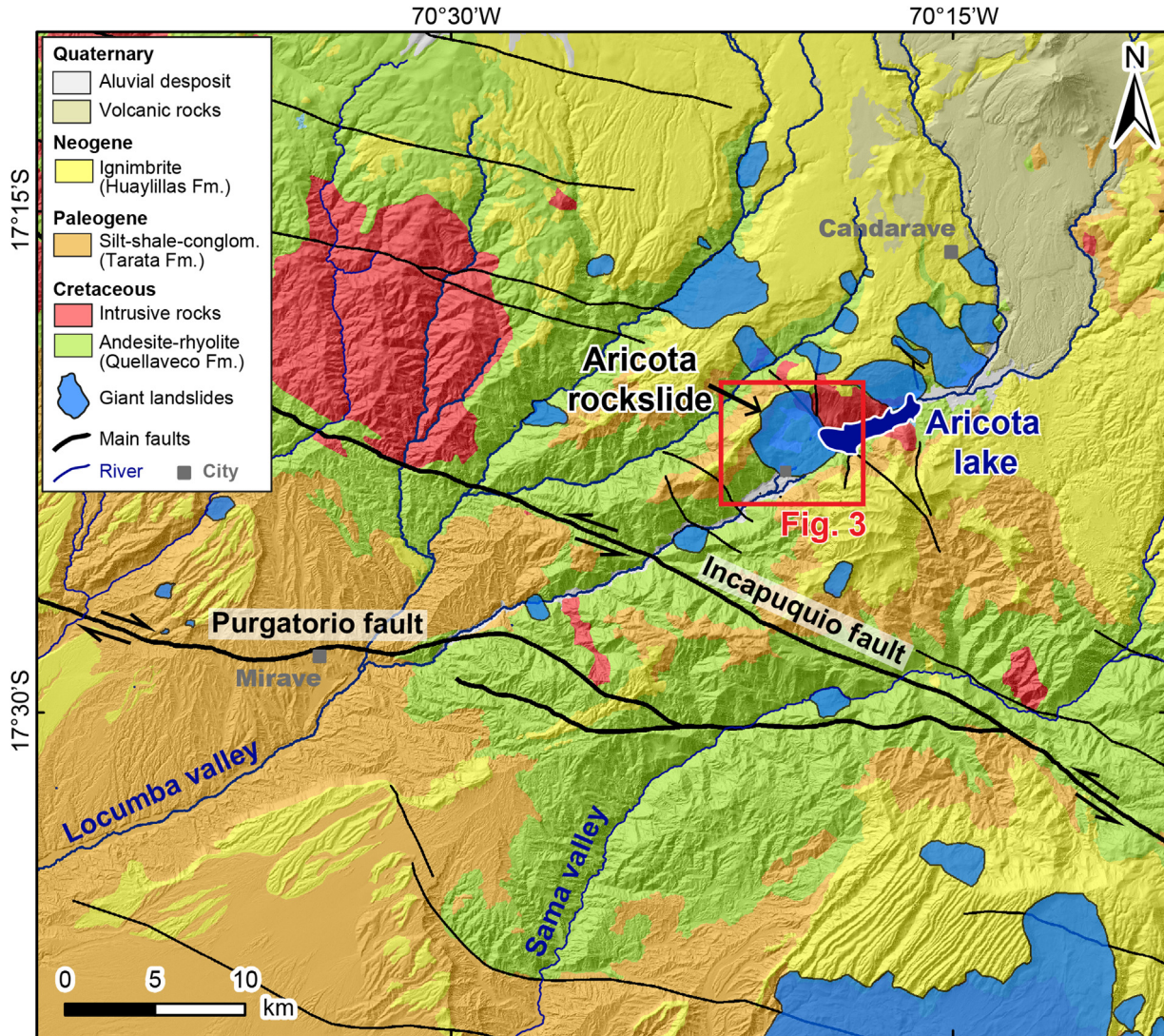


Fig. 2. Geological settings around the Aricota rockslide (see frame location on [Fig. 1](#)). The geological map is adapted from INGEMMET (2011) and draped above hillshade produced using the TanDEM-X DEM (resolution 12 m). Quaternary crustal faults are reported (e.g. Incapuquio-Purgatorio fault system; [Hall et al., 2012](#); [Benavente et al., 2017](#)). Giant landslides reported were mapped during this study.

rate ($\pm 0.4 \text{ mm.ka}^{-1}$) and attenuation length ($\pm 10 \text{ g. cm}^{-2}$). Total age uncertainties (i.e. external) include contributions from the analytical method and production rate uncertainty ([Marrero et al., 2016](#)). All results are presented in Table 1 (supplementary data).

4. Results and interpretations

4.1. Rockslide morphology

The failure of the Aricota giant rockslide has left a spectacular morphological imprint in the Locumba valley and has deeply modified the surrounding landscapes ([Figs. 3–4A](#)). It generated a natural dam of about 600 m of height impounding a lake of $\sim 0.8 \text{ km}^3$ with a length of $\sim 6 \text{ km}$ (Aricota lake) and produced a large scar of about 4 km of width along the northern flank of the valley ([Fig. 3A](#)). As it is visible on the [Fig. 3A](#), the main scarp intercepts a plateau, corresponding to a paleo ignimbrite surface (Huayllillas formation, [Fig. 2](#)), at an elevation of ca. 3700 m a.s.l. According to the geomorphological description proposed by [Placzek et al. \(2001\)](#), two successive deposits can be distinguished in the rockslide mass. The dam itself and a subsequent rock-avalanche deposit overlying

its northern part. The whole destabilized area extends over $\sim 3 \text{ km}$ of length towards the south until the opposite valley slope.

We observe in the central part of the dam a continuous lithological succession, locally fractured, composed from bottom to top by the Huayllillas ignimbrites ([Fig. 5A](#)), overlying the metasediment (silts-shales) and pyroclastics of the Tarata formation. This lithological succession is comparable with the one outcropping along the stable valley slopes ([Figs. 3B and 4](#)). On southern extremity of the dam (i.e. the most distal part), we observe a dominance of andesite from the Quellaveco formation ([Fig. 3B](#)), derived from the lower most layer of the original slope, with a high degree of destratification, also mixing all the other lithologies ([Fig. 4B](#)). According to those observations, the dam was likely produced during a first large and “in mass” rockslide failure that have affected the whole valley flank.

The western side of the dam (downstream side) shows a large amphitheater ([Fig. 3A](#)), affected by gullies and landslides with scars of several hundred meters in length ([Fig. 6A](#)). Water seeping is also observable at the base of the dam (see location of current and paleo springs on [Fig. 3B](#)). We interpret this morphology as regressive erosion processes affecting the dam due to its steep topography and to the high level of rock fracturing produced during the rock-

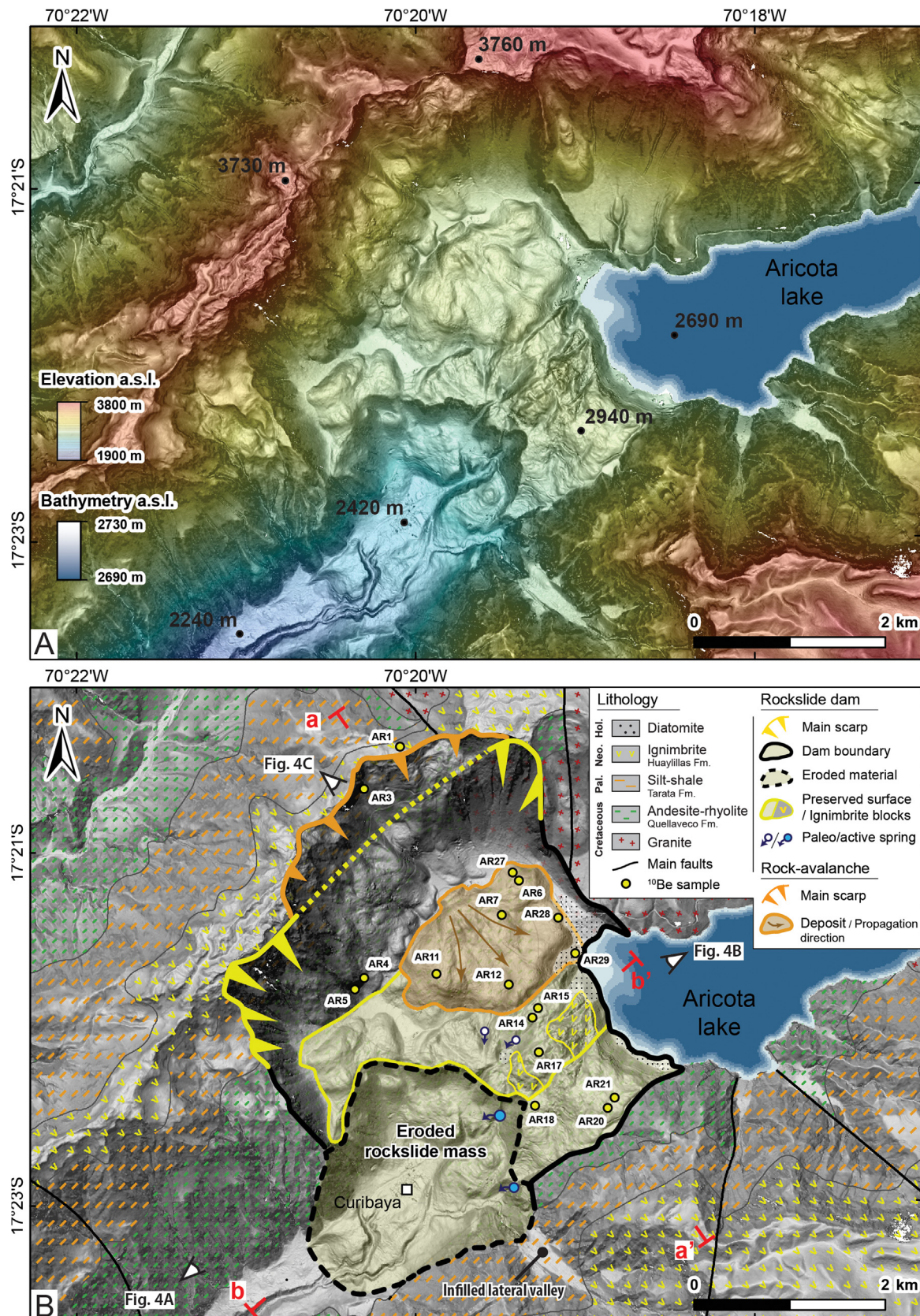


Fig. 3. The Aricota giant rockslide (see frame location on Fig. 2). (A) Raw hillshade and elevation image derived from high resolution (2 m) Pléiades DEM (see text for details). The bathymetry of the Aricota lake (resolution 1 m) has been provided by the company EGESUR. (B) Geomorphological map of the Aricota rockslide showing the two failure events. The first and main event that generated the dam in the valley is mapped in yellow. Note the regressive erosion affecting southwestern part of the slipped mass and the infill of the secondary valley located at the southern center of the map. The second event, a rock-avalanche that have affected the main scarp of the first event, is depicted in orange. Yellow points correspond to samples extracted for ^{10}Be cosmic ray exposure dating (1 above the rockslide scarp, 3 on the free face of the rockslide scarp and 13 on boulders distributed over the landslide mass). Outside of the rockslide area, the geology is the same as Fig. 3.

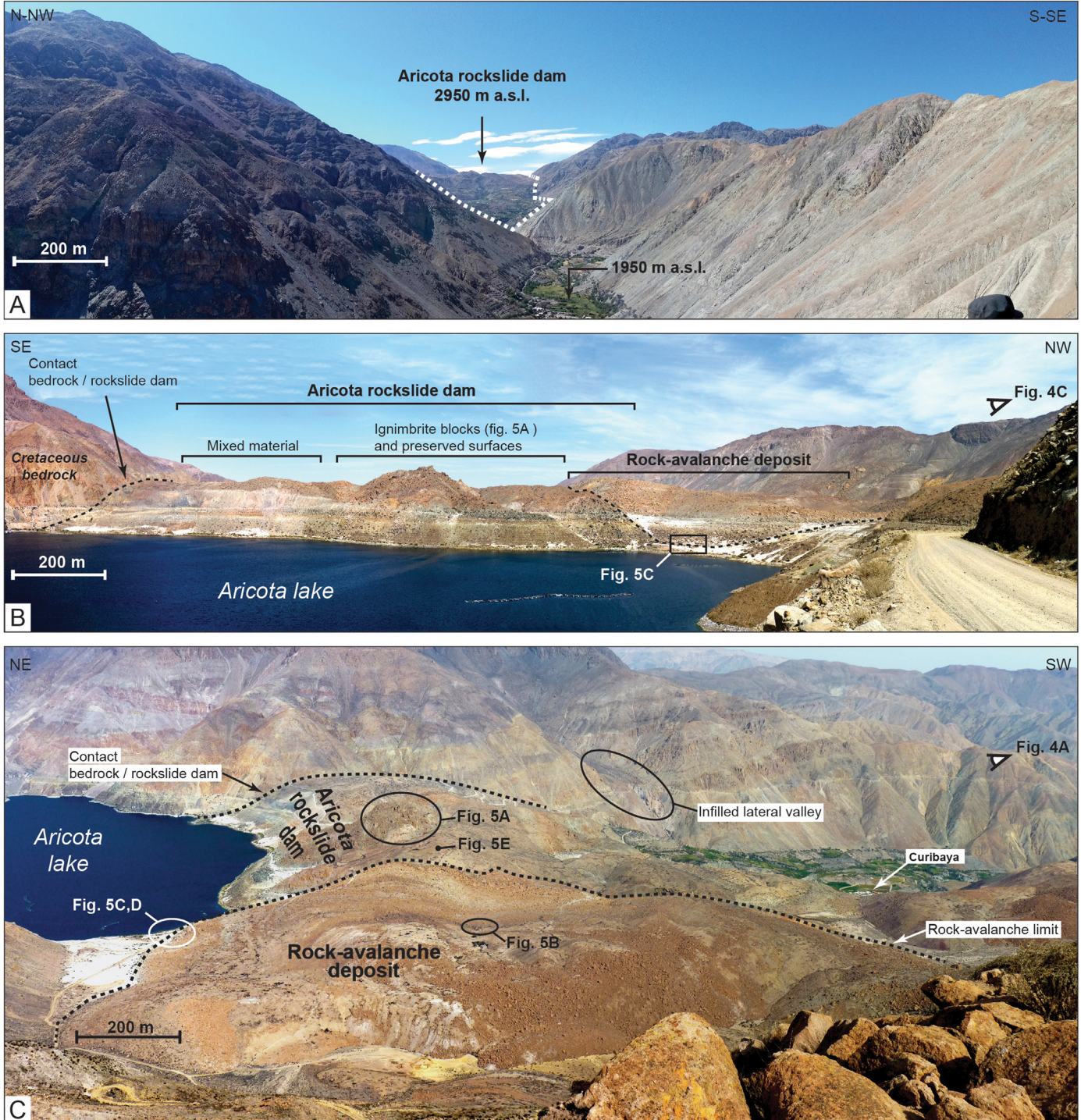


Fig. 4. Panoramic views illustrating the main structures of the Aricota giant rockslide area. (A) Panoramic view from the downstream part of the Locumba valley (see location on Fig. 4C). Note the general V-shape of the valley and the contact between the giant Aricota rockslide and the flank underlined by a dotted white line. (B) Westward view taken from the road along the lake (see location on Fig. 3B) and showing the dam generated by the first giant event. Along the dam, two bodies can be discriminated. On the central part, pre-rockslide topographic surfaces and large ignimbrite blocks are preserved (see also Fig. 5A). On the south-eastern part, mixed and highly deformed material are outcropping. Rock-avalanche deposits overlie the top the rockslide dam. (C) Southward view of the whole rockslide area taken from the top of the scarp (see location on Fig. 4B). Note on the opposite Locumba valley flank, the lateral valley infilled by accumulation of deposits reflecting its obstruction by the main Aricota rockslide dam.

slide propagation. On the opposite Locumba valley flank (southern flank), our DEM (Fig. 3A) highlights a flat and perched surface, at the same elevation than the Aricota dam (ca. 2700–2800 m a.s.l.), infilling a small lateral valley (Fig. 4C). This morphology suggests that the former dam reached this area before being eroded.

Postulating that before the rockslide triggering, the valley had a typical v-shaped morphology (Fig. 4A) we reconstructed a pre-

failure topography. Then taking into account the strike and dip of the main scarp, we estimate a volume of ca. $2 \pm 0.3 \text{ km}^3$ for the Aricota rockslide dam, which includes an estimation of the volume eroded since it emplaced.

On its northern part, the dam is covered by a secondary rock-avalanche deposit constituting a circular lobe of debris of 800 m of radius (Fig. 3A). The contact between the dam and this rock-



Fig. 5. Detailed morphologies of the Aricota rockslide. (A) Preserved large ignimbrite boulders outcropping in the central part of the rockslide dam. (B) Large boulders from the Tarata formation (bedded silt and shales) aligned in the rock-avalanche deposit. (C) Boulders of the rock-avalanche partially covered by diatomite. This zone was immersed before the hydroelectric lake drop. (D) Boulder (AR29) sampled to tentatively tract the paleo-lake level variations. (E) Boulder of sample AR15. (F) Ignimbrite surface located on the plateau at the top of rockslide scarp and sampled to estimate the long-term local denudation rate (see location on Fig. 3B). On all pictures, see the persons for scale and their location on Fig. 4.

avalanche deposit is delineated on the DEM by a slope break (Fig. 3). On the field, it corresponds to a clear contact between a chaotic deposit of blocs of thickness of 60 to 100 m overlying the oldest dam surface. Taking into account the area covered by the rock-avalanche and its mean thickness; we estimated a volume $\sim 0.2 \text{ km}^3$ for this

second event. Above this rock-avalanche deposit, we observe a high cliff of more than 200 m of elevation, cutting through the intercalations of silts and shales from the Tarata formation (Fig. 6C). This cliff crosscuts morphologically the main scarp left by the first fail-

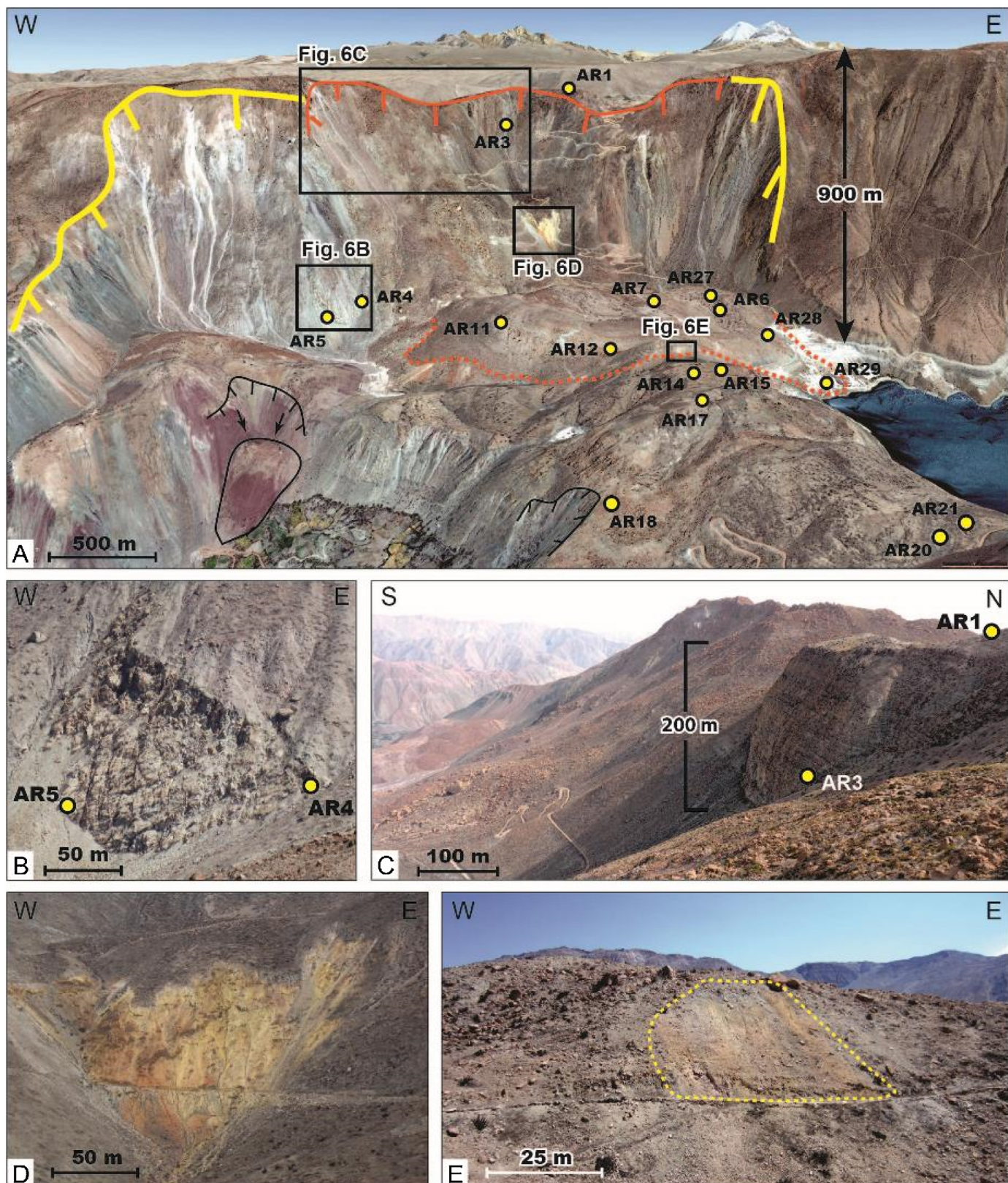


Fig. 6. Main scarp morphologies of the Aricota rockslide. (A) 3D view of the Aricota rockslide area (Google Earth). The scarp of the rockslide dam (first event) is depicted in yellow while the rock-avalanche scarp (second event) is in orange. Dashed orange line highlights the boundary of the rock-avalanche deposit. Small landslides (in black) affect the southwestern slope of the rockslide dam. (B) Preserved scarp surface of the first failure event and location of samples AR4 and AR5. (C) Vertical scarp generated by the second failure event and cutting through alternating silts and black shales of the Tarata formation. Sample AR3 was extracted from the scarp toe. See also location of the sample AR1 at the top of the slope, dedicated to constrain long-term denudation rate. (D) Layer corresponding to a regional paleo weathering profile interbedded in Cretaceous series. (E) Same weathered material (yellow) reworked and transported by the rock-avalanche.

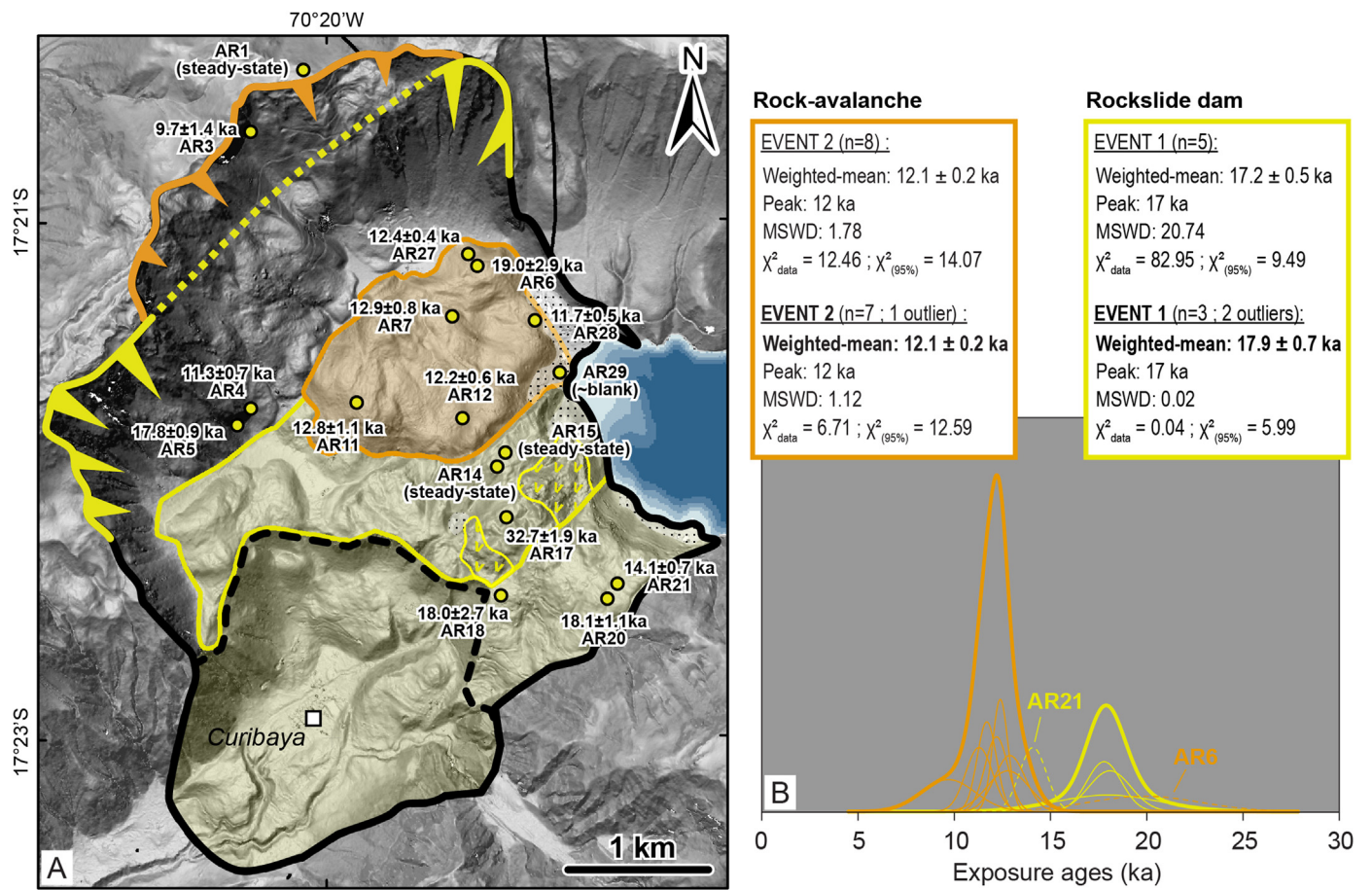


Fig. 7. Exposure durations results on the Aricota giant rockslide. (A) Rockslide map and sample ages (1σ internal uncertainty, Table 1, supplementary data). Legend is the same as Fig. 3B. (B) Probability density plot and statistics over exposure durations (1σ internal uncertainty, Table 1, supplementary data). Yellow curves and orange curves correspond to the rockslide dam (event 1) and the rock-avalanche (event 2), respectively. Thin lines correspond to individual exposure durations. Dashed lines refer to exposure durations interpreted as outliers (see text for details). Exposure duration from sample AR17 (32.7 ± 1.9 ka) is considered as an outlier (out of frame). Thick curves refer to the summed probability density function for each event (excluding outliers).

ure over a width of ~3 km (Figs. 3B and 6 A) inducing a regression toward the north of about 600–700 m.

Two types of structures can be distinguished in the rock-avalanche deposit. The firsts ones correspond to radial structures in the morphology (Fig. 3A), which directions point mainly toward the southeast. They are interpreted as an indication of the main direction of debris propagation toward the southeast. The second types of structures are concentric and are revealed by several bands of colors (black, brown and white) that are alternating in the deposit (Fig. 4C and Fig. 6A). Those colors correspond to different lithology of boulders. Indeed, from the northern to the southern part of the deposit, we can recognize boulders of ignimbrite and weathered material from the Huayllilas formation, followed by alignment of black silt-shale boulders from the Tarata formation (e.g. Fig. 5B) and finally very large boulders (up to 25 m in length) of andesitic breccia from the Quellaveco formation. The eastern side of the rock-avalanche deposit is composed of granitic boulders such as they outcrop above and along the top of the scarp (Fig. 3B). At the front of the rock-avalanche deposit (Fig. 6A), we observed an outcrop of weathered yellow material that originates from the middle part of the upper slope (Fig. 6D).

As a whole, those morphologies and such spatial distribution of boulders indicate that the former lithological succession of the slope was not mixed during the rock-avalanche and debris transport. The failure mode probably follows a translational failure allowing the bottom part of the slope to be projected in the distal part of the deposit.

4.2. Denudation rate and exposure duration results

Denudation rate and exposure durations derived from ^{10}Be data are reported in Table 1 (supplementary data). As previously mentioned, our first objective was to constrain the local denudation rate of the Aricota rockslide area in order to derive accurate exposure durations. The sample AR1, extracted on the ignimbritic plateau for this purpose, provided a high concentration of $38.00 \pm 1.36 \times 10^5$ at. g $^{-1}$. This indicates a saturation of ^{10}Be , i.e. a steady state, which is reached after an exposure duration greater than 1 Ma (Gosse and Phillips, 2001) at this latitude and elevation (17°S and ca. 3700 m a.s.l.) and corresponds to a denudation rate of $3.1 \pm 0.6 \text{ mm.ka}^{-1}$. Unexpectedly two other samples, AR14 and AR15, taken at the top of the Aricota rockslide dam also provided steady-state concentrations of $43.78 \pm 1.42 \times 10^5$ and $50.49 \pm 1.47 \times 10^5$ at. g $^{-1}$, corresponding respectively to denudation rates of 2.6 ± 0.5 and $2.2 \pm 0.4 \text{ mm.ka}^{-1}$. The presence of those steady-state surfaces in the main rockslide body suggests that a part of the original topography of the plateau was preserved during the mass movement. The implications of that result for the understanding of the failure typology will be more specifically discussed hereafter. All agreeing within uncertainties, those three denudation rates success a chi-2 test (1.39/5.99 (95%)) and belong to the same population whose weighted mean is $2.6 \pm 0.4 \text{ mm.ka}^{-1}$ (uncertainty attached is 1 sigma weighted standard deviation).

Exposure durations were then calculated using this mean denudation rate. In general, as shown on the Fig. 7B, exposure dura-

tions obtained are in good agreement with the geomorphological settings and they allow discriminating the two successive events that occurred on the Aricota rockslide. In the following, the exposure durations are reported with one sigma internal uncertainty.

The youngest exposure durations correspond to boulders of the rock-avalanche deposits, corresponding to the second event. Five exposure durations over six (samples AR7, AR11, AR12, AR27 and AR28) range between 11.7 ± 0.5 and 12.8 ± 1.1 ka (Table 1 (supplementary data) and Fig. 7B). The sample AR6 (19.0 ± 2.9 ka) is the only one age of this lobe of deposit falling out of this range, and for which we suspect likely inheritance. Comparing with exposure durations of ca. $12\text{--}13$ ka, the excess of ^{10}Be concentration in this sample would be about 1×10^5 at. g $^{-1}$. Along a depth profile that is theoretically at the equilibrium, and considering the denudation and the production rate conditions of the plateau (mean denudation rate of 2.6 ± 0.4 mm.ka $^{-1}$, “infinite” time, and production scaling of sample AR1), this concentration would be achieved at depth of 4 to 6 m. It is thus probable that the boulder AR19 comes from this pre-failure depth location and then was deposited in the debris with non-zero initial ^{10}Be concentration, giving an apparent older exposure duration. The sample AR3, picked at the foot of the vertical scarp located directly above the debris lobe (Fig. 6A and C), provided an exposure duration of 9.7 ± 1.4 ka, not significantly different from the previous ones considering the uncertainties. It confirms the relation between this secondary scarp and the rock-avalanche deposits.

Finally, the sample AR4, that was extracted from the northern part of the scarp presented on Fig. 6B (see also location on Fig. 3B), provided an exposure duration of 11.3 ± 0.7 ka that also agree with the one's previously listed. It is likely that the rock-avalanche failure has rejuvenated this side of the main scarp during its propagation. A probability density plot including all those samples (Fig. 7B) highlights a unimodal distribution (chi-2 test (95%): 6.71/12.59), the weighted mean of which is 12.1 ± 0.7 ka (uncertainty attached is 1 sigma weighted standard deviation). Considered or not, the AR4 and AR6 samples do not affect the result (Fig. 7B).

Exposure durations obtained from the five samples picked on the dam area (AR5, AR17, AR18, AR20, AR21), and its corresponding scarp, are significantly older. They range between 14.1 ± 0.7 and 32.7 ± 1.9 ka (Table 1, supplementary data). The probability density distribution provided on Fig. 7B shows that three of those ages (AR5, AR18 and AR20) agree within uncertainties (chi-2 test (95%): 0.04/5.99) and point to a weighted mean of 17.9 ± 0.7 ka. Inheritance is inferred in the sample AR17 (32.7 ± 1.9 ka) leading to a significantly older apparent exposure duration than the mean duration. This is fairly concordant with the fact that (1) the sample AR17 was extracted on boulders close to the samples AR14 and AR15 at steady state, and (2) all those samples are all standing in an area of preserved surface (Figs. 3B and 7) representing pre-rockslide topography.

The ^{10}Be concentration of sample AR21 (14.1 ± 0.7 ka) leads to a significantly younger apparent exposure duration. We interpret this younger apparent age as the consequence of a desquamation process of the boulder surface following the typical onion-skin weathering of the Atacama desert.

We measured in the sample AR29 (Fig. 5C and D) a $^{10}\text{Be}/^{9}\text{Be}$ ratio of $0.56 \pm 0.08 \times 10^{-14}$ that is equivalent to the corresponding blank value for this run ($0.52 \pm 0.23 \times 10^{-14}$, Table 1, supplementary data). This means that the ^{10}Be concentration in this sample is close to the detection limit, implying an exposure duration close to zero. The Fig. 8 shows the morphological context of the boulder AR29. It stands at an elevation of 2760 m, while the pre-1967 level was at 2790 m and the highest level deduced from diatomite deposit (Placzek et al., 2001) was estimated at ca. 2830 m (Fig. 8B). As this boulder belongs morphologically to the second event (mean age of deposition is 12.1 ± 0.7 ka), its very low ^{10}Be concentra-

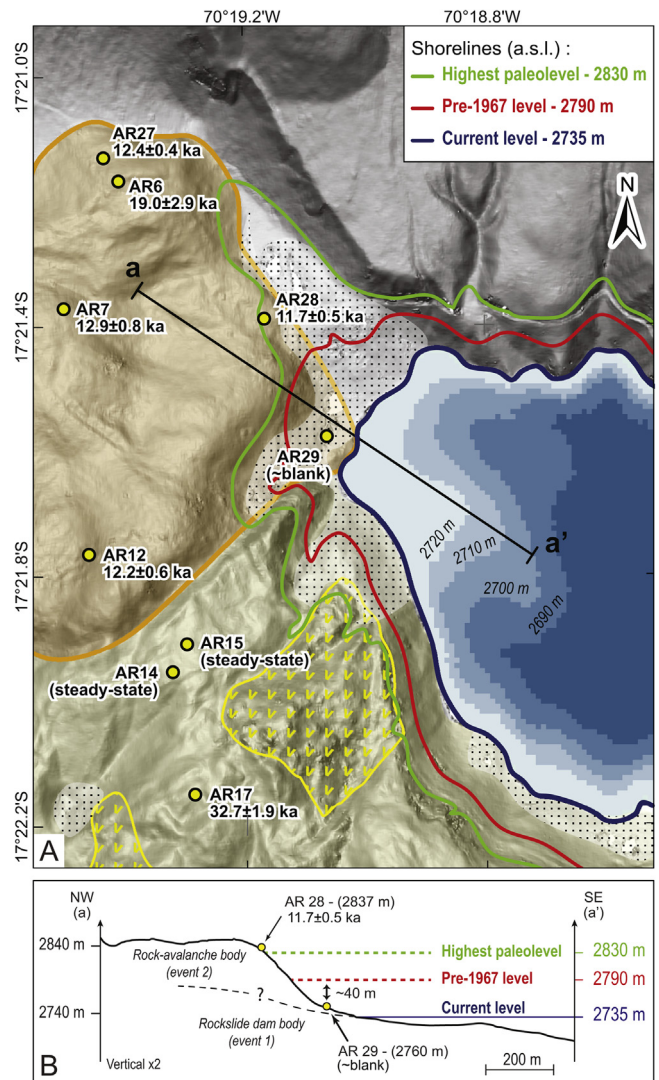


Fig. 8. Morphological context around the sample AR29. (A) Geomorphological map of the north-eastern part of the Aricota dam showing the location of the sample AR29 and the main variations of the Aricota lake shorelines (the probable highest paleo-lake level was reconstructed according to diatomite deposits (Placzek et al., 2001)). (B) Topographic profile extracted from the Pléiades DEM (see location on Fig. 8B). The legend of the rockslide morphologies is the same as Fig. 3B.

tion suggests that during the rock-avalanche, the boulder likely fell directly in deep water, thus shielded from the incident cosmic ray particles up to now.

5. Discussion

Most of the large landslides identified in the Central Western Andes, including the Aricota rockslide, have developed along the flank of deeply incised canyons (Fig. 1; e.g. Crosta et al., 2014; Thouret et al., 2017). In those canyons, the incision can locally exceed 1500 m (Thouret et al., 2017) suggesting that the topography is probably the first preconditioning factor for those giant gravitational failures. The same conclusions were made by Strasser and Schlunegger (2005), and Wörner et al. (2002) regarding the Lluta landslide. The deep incision of those canyons is the result of the peculiar conditions prevailing along the Central Western Andes since several millions of years (Schlunegger et al., 2006; García et al., 2011; Gunnell et al., 2010; Bissig and Riquelme, 2010; Jeffery et al., 2013). It is first related to the uplift of the region since the Cenozoic (e.g. Schildgen et al., 2009; Thouret et al., 2007). Second, it is related

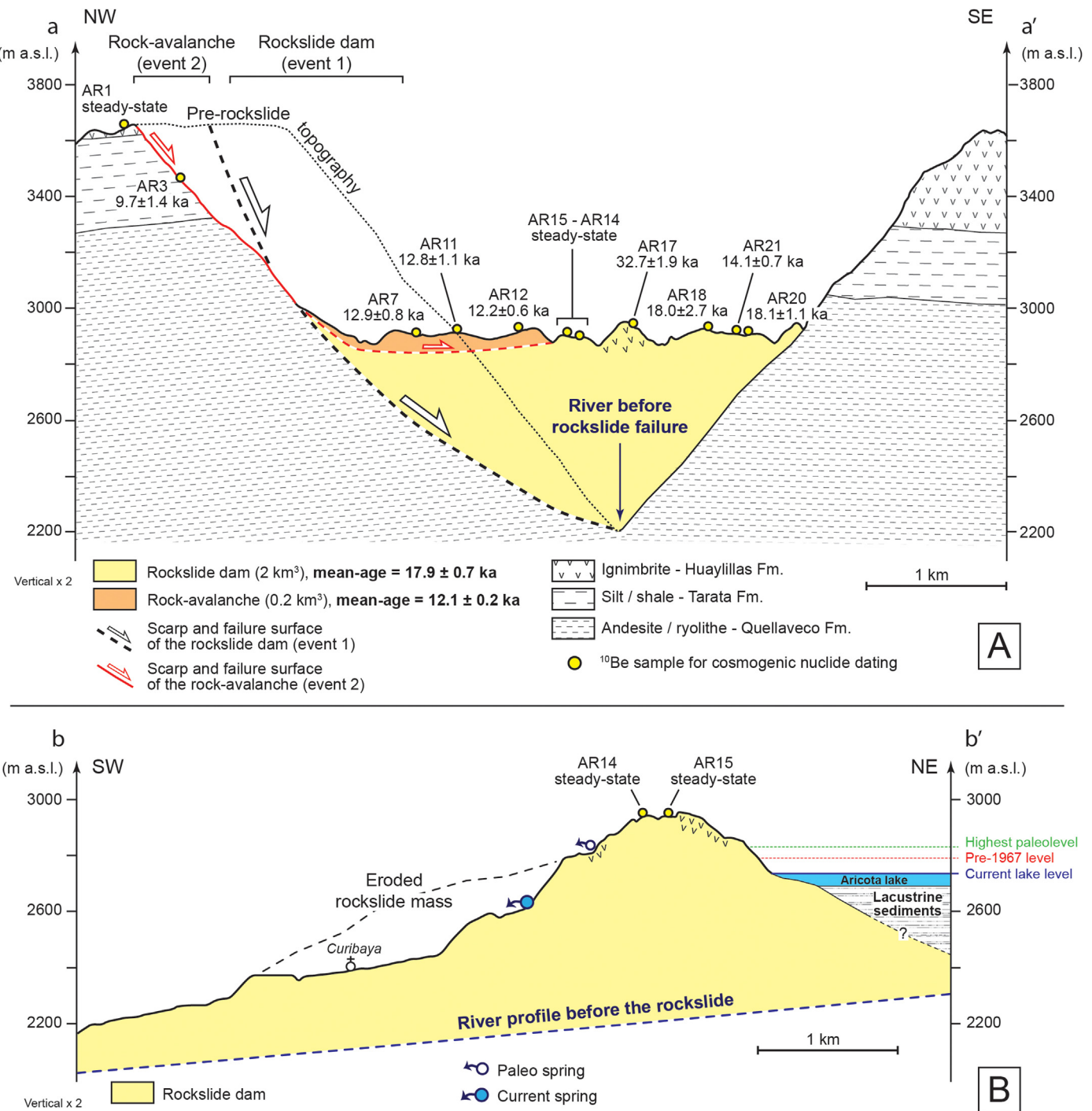


Fig. 9. Interpretative cross-sections of the Aricota giant rockslide. See locations on Fig. 3B. (A) Perpendicular to the Locumba valley. The pre-rockslide topography, before the first event, is reconstructed considering the volume estimation of the rockslide dam and interpolating the slope of the valley flanks (Delgado et al., 2018). Samples for ^{10}Be cosmic ray exposure dating are projected on the cross-section. (B) Parallel to the Locumba valley. The pre-rockslide dam river profile is indicated from Delgado et al. (2018).

to the specific climate condition marked by a long lasting hyper-aridity affecting all the Central Western Andean flank (Atacama desert) until elevations of about 3000 m a.s.l., and, on the other hand, precipitations from the easterlies that reached the upper part of the western watersheds (Altiplano and Western Cordillera). Indeed, after Huffman et al. (2007), while current mean precipitation are $\sim 0 \text{ mm/yr}$ along the coast and the Western Cordillera, about 800 mm/yr of precipitation in average are recorded on the Altiplano. This rain shadow effect started possibly at 12/10 Ma (e.g. Ehlers and Poulsen, 2009; Insel et al., 2012; Rech et al., 2019). This

way, while the western flank of the Andes remains hyper-arid, the upper catchments collect a significant amount of water, flowing then throughout the Cordillera toward the Pacific (Litty et al., 2017). This discharge has maintained a constant incision in the valleys thus contributing to maintain very steep canyon flanks and critical topographic wedges highly prone to large-scale landslide failure (Thouret et al., 2017). As it was globally reported by Korup et al. (2007), and locally by Wörner et al. (2002) in the Lluta valley, this suggests that the critical relief (see also Blöthe et al., 2015) that can be close, or even beyond, to its proposed upper strength limit may

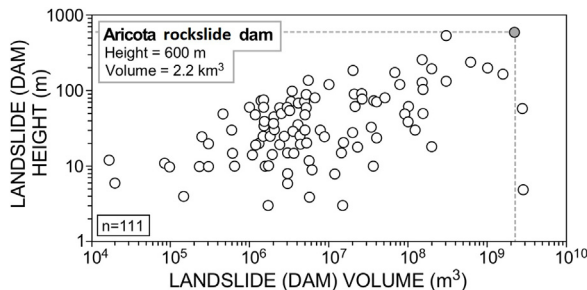


Fig. 10. Worldwide compilation of landslide dams modified from Korup et al. (2004) showing the relations between the landslide volumes and heights (n is the number of landslides of the database). The Aricota rockslide (grey circle) stands within the 3 largest landslide dams and the highest height reported worldwide.

be one of the primary factor controlling the development of large landslides in the Andean canyons.

In the Locumba valley, the gravitational failure of the canyon flank was deep and large enough to produce a massive dam generating upstream a lake more than 6 km long. As shown by our morphological analysis, two successive failure events occurred at the Aricota site (Fig. 3 and Fig. 9). A first main event, of rockslide typology, created the dam and then a second event occurred, of rock-avalanche typology, which deposits spread out on top of the first ones, reinforcing the initial dam. Taking into account the height of the dam (~ 600 m), its volume ($2 \pm 0.3 \text{ km}^3$) and the pre-rockslide valley morphology, we propose that the first event (rockslide dam) has affected the ignimbritic plateau over a maximal width of 400–500 m (Fig. 9A). The failure allowed the collapse of a part of this plateau originally located at ca. 3650 m a.s.l. Ignimbritic rock volume outcrops at the present-day at the top of the rockslide dam at ca. 2900 m a.s.l. (Fig. 9A). Translational movements probably dominated the failure type as the vertical distribution of the stratigraphy is preserved in the dam. This morphological characteristic has been already described in various study cases of large slope destabilizations (Shreve, 1968; Strom, 2006; Humair et al., 2013). According to the classification of Hermanns et al. (2011), the distribution of the Aricota rockslide deposits in the Locumba valley corresponds to a type "IV a" in plan view. Indeed, the run-out of the debris was long enough (~ 3 km) to reach the opposite valley flank and to dam a small tributary valley (Fig. 3). As shown on the geological cross-section Fig. 9A, along a cross-valley profile, the deposit profile is roughly flat and symmetric to the original valley profile. This would correspond to a type "i" of cross-valley profile in the classification of Hermanns et al. (2011). The cross-section of the rockslide deposit, parallel to the valley (Fig. 9B), highlights the large thickness of the dam (600 m) and shows similarities with the type "2" of the along-valley profile classification of rockslide dams that is associated with a large lake (Hermanns et al., 2011). The great depth of the failure surface and the confined setting of the original Locumba valley may explain the high thickness of the deposit (Fig. 9B).

As shown on Fig. 10, comparing with the compilation of landslide dams established by Korup (2004), the Aricota rockslide dam stands among the largest worldwide. To explore the geotechnical stability of this dam, we compiled the two indexes developed by Casagli and Ermini (1999). They are based on geomorphometric parameters of the site: (1) the Blockage Index $I_b = \log(V_D * A_C^{-1})$ and (2) the Impoundment Index $I_i = \log(V_D * V_L^{-1})$, where V_D and V_L are the volumes of the rockslide dam and the lake [in m^3], respectively, and A_C is catchment area upstream of the blockage [in km^2]. The values obtained for the Aricota rockslide dam are $I_b = 6$ and $I_i = 3.4$ (taking $V_D = 2 * 10^9 \text{ m}^3$, $A_C = 1600 \text{ km}^2$ and $V_L = 8 * 10^5 \text{ m}^3$ (Placzek et al., 2001)) indicating the stability of the site. Indeed Korup et al. (2004) shown that below $I_b = 2$ no landslide-dammed lakes formed,

whereas unstable lakes form at $I_b < 4$ and that impoundments with $I_b > 7$ have remained stable. Similarly, sites where $I_i > 1$ have all retained existing lakes, whereas locations with $I_i < 1$ comprise both stable and unstable landslide dams. Since the dam emplacement, the progressive infilling of the lake by lacustrine sediments (Fig. 9B) have also decreased the water volume and therefore reduced the pressure imposed to the dam. More generally, megatsunami is another hazard potentially linked to mountain lakes (either natural, landslide dam or artificial lakes) that can be triggered by slope failures around the lake (Hermanns et al., 2004). Taking into account the steep slope around the Aricota lake, this hazard cannot be excluded and deserve to be studied.

In the case of large landslide processes, Glade and Crozier (2005), or Hermanns et al. (2006) introduce that both preparatory factors (static and dynamic) and triggering factors are often interdependent and play crucial role in the slope failure evolution. In our study the geomorphological observations combined with cosmogenic nuclide dating obtained on the Aricota rockslide area show clearly two stages of destabilization at 17.9 ± 0.7 ka and 12.1 ± 0.2 ka, corresponding to the main rockslide dam event and to the secondary rock-avalanche, respectively (Fig. 9A). This timing of events provides a frame to discuss the nature of forcings that may have triggered the two slope failures. However, we do not have any constraints to discuss the preparatory phases and their related factors, thus the following discussion focuses on triggering factors only.

According to the literature, most of the contemporaneous, or historical landslide dams, have been triggered by earthquakes. Some of the most impressive cases are the Usoy landslide (volume = 2.4 km^3 , impounding a lake of a 17 km^3), triggered in 1911 by an earthquake of Mw7.7 (Ambraseys and Bilham, 2012), the Tortum landslide (0.18 km^3) in Turkey (Duman, 2009), or the numerous landslide dams in southeastern Italy which triggered by earthquakes of intensity VII to X during the 17th (Nicoletti and Parise, 2002). In the Andes, mostly in the NW Argentina, numerous paleo-landslide dams were reported and attributed also to past earthquakes (Wayne, 1999; Hermanns and Schellenberger, 2008; Moreiras et al., 2015).

Considering that the Aricota rockslide is located in a tectonically active region, with two large crustal fault systems (Incapuquio and Purgatorio faults) located from 10 to 20 km south of the rockslide (Fig. 2), a coseismic triggering of the Aricota slope failures is probable. Indeed, Benavente et al. (2017) revealed Holocene seismotectonic activity of the Purgatorio fault, showing at least two ruptures of ~ 3 and ~ 2 m of vertical offset at the surface, equivalent to $> \text{M}_w 7$ shallow seismic events. However, even if those faults represent high seismogenic potential in the close field of the rockslide, it does not exist for the moment any paleoseismic records as old as the Aricota slope failures that would corroborate a coseismic trigger. Another observation is that several landslides, including the Aricota ones, seem to cluster spatially on the hanging wall of the Incapuquio fault (transpressive senestral, Fig. 2). Similarly to what was reported by Gorum et al. (2011) in the Sichuan after the 2008 Wenchuan earthquake, such a landslide distribution could reflect a coseismic "hanging wall" effect. Indeed, Gorum et al. (2011) noticed that most of the landslides triggered during the Wenchuan earthquake occurred on the hanging wall block of the Wenchuan-Maowen fault. This massive landslide triggering was interpreted as a site effect and a probable amplification of ground motion in this area (Chiou and Youngs, 2014). Over the long-term, a higher concentration of slope failures on the hanging wall of the Incapuquio fault (Fig. 2) can be interpreted also as the effect of the river incision into the uplifting block, which may have increased and steepened the relief there.

On the other hand, several studies reported that in northwestern Argentinian Andes many landslide producing dammed lakes may have formed during wet periods (e.g. Trauth et al., 2003). Moreiras

and Sepúlveda (2015) provide an up-to-date inventory of mega paleolandslides in the Central Andes at 32–34°S and discuss traditional hypotheses used to explain landslide occurrences. Whereas earthquakes have been widely proposed as the main triggering mechanism of the Chilean slope failures, paleoclimatic conditions are considered as the main cause of mega-landslides in Argentina. However, Moreiras and Sepúlveda (2015) also insist on the fact that local evidences and geological records of those wetter periods are often lacking. On our study area at 17°S, it is striking to note the synchronicity between the chronic of failures of the Aricota rockslide and the two latest humid periods recorded at the scale of the Central Altiplano since 20 ka, pointing to a potential climatic control on the Aricota rockslide triggering. Those humid periods, documented since the 80°S' (e.g. Blodgett et al., 1997), are characterized mainly by two major expansions of the Altiplano lakes: the Tauca (18.5–14.5 ka) and the Coipasa (12.8–11 ka) phases (Placzek et al., 2013), during the Heinrich Stadial 1a and the Younger Dryas, respectively. Recently Martin et al. (2018) explored in details the past climate conditions during the Tauca phase by simultaneously reconstructing the fluctuations of lake levels and glacier advances in the Altiplano region. They found that during this period, on the northwestern edge of the Altiplano and the upper Locumba basin, the paleoprecipitations were amplified by 2–3 times compared to the present day precipitation. At a regional scale, the occurrence of such drastic increases of the paleoprecipitation is corroborated also by the concomitant aggradation of alluvial terraces and fan systems on valley floors along the western Peruvian margin. For instance, in the Majes river, located at about 300 km northwest to the Locumba valley, Steffen et al. (2010) pointed to the occurrence of major periods of aggradation at ca. 20 ka and between 12–8 ka. In the Moquegua valley (50 km northwest to Aricota), Keefer et al. (2003) reported the existence of extensive flood and debris flow deposits dated between 12 and 8.4 ka, and at least ten severe events that took place between 38 and 13 ka. At a larger scale along the western margin of the Andes in Peru, Litty et al. (2017) highlighted changes in precipitation patterns during the last 100 ka through shifts of the sediment provenance. In the Pisco valley, 700 km northwest to the Locumba valley, Steffen et al. (2010) and Bekaddour et al. (2014) conclude that phases of sediment aggradation and accumulation were triggered by shifts toward a more humid climate conditions during the Tauca paleolakes maximal expansions.

As a summary, several lines of evidences point toward significant increase of paleoprecipitation regime along the Central Western Andes during the periods 18.5–14.5 ka and 12.8–11 ka (Placzek et al., 2013). Given the correlation between those wet events and the timing of the Aricota rockslide (17.9 ± 0.7 ka and 12.1 ± 0.2 ka, Fig. 7); we tentatively propose that the generation of catastrophic mass movements in the Locumba valley was firstly climatically driven. Prolonged periods of increased precipitation may have reduced thresholds for slope instabilities by increasing water content in the unstable masses, decreasing the effective friction over the sliding planes, and eroding slope foots because of higher river discharge.

6. Conclusions

In this paper, we provide a geomorphological analysis and dating of the Aricota giant rockslide, located in the Central Western Cordillera of southern Peru (17°S). Our results indicate the occurrence of two successive events. A giant failure producing a rockslide dam occurred first at 17.9 ± 0.7 ka. This first destabilization event mobilized a rock volume of ca. 2 km^3 and affected the northern flank of the Locumba valley. As shown by the presence of large preserved ignimbrite blocks overlying mixed and fragmented material in the dam, this first failure event was “in mass”. It gener-

ated an impressive dam in the main valley with a height of about 600 m, impounding a lake of approximately 6 km long upstream that remains until today. At 12.1 ± 0.2 ka, a second event of destabilization cross-cutting the initial scarp produced a rock-avalanche of ca. 0.2 km^3 which debris spread out at the top of the northern part of the dam formed by the first event. The chronology of those two events of destabilization is compatible with the main paleoclimatic events of this region during the Heinrich Stadial 1a and the Younger Dryas, both characterized by paleoprecipitation increases. Furthermore, aggradation of alluvial terraces and fan systems are concomitant along the valley floors of the western Peruvian margin highlighting higher regional erosion, sediments supply and mass-wasting events during those two periods. This temporal correlation suggests that the climate has played a preponderant role on the triggering of the Aricota rockslide. However, additional and/or concomitant effect of crustal earthquakes on the rockslide initiation cannot be ruled out considering the seismotectonic setting of this Andean region. Future studies related to paleoseismicity would help to clarify this debated question. At the scale of the Central Andes, although numerous giant paleolandslides are recognized on its western arid flank, their understanding still suffers of a lack of time constraints, either in term of climatic events or in term of their individual geomorphic description.

Declaration of Competing Interest

The authors declare that they have no known competing financial interests or personal relationships that could have appeared to influence the work reported in this paper.

Acknowledgments

All the data used to perform this study are available in the paper and in the supplemental material. This research is part of the agreement between IRD and INGEMMET. It was financially supported by IRD and INGEMMET (Neotectonics program), a grant from Labex OSUG@2020, the French National Research Agency in the framework of the “Investissements d’avenir” program (ANR-15-IDEX-02 and ANR10 LABX56) and the CNES through the program TOSCA. The Astrium and the ISIS/CNES program provided the Pléiades images. The authors acknowledge Pascal Lacroix for his support during the Pléiades images processing. The company EGESUR is thank for having sharing the bathymetry data of the Aricota lake. The sample processing and chemical extraction of the ^{10}Be were performed at the GTC plateform (ISTerre, Grenoble). We gratefully thank Francis Coeur for the sample processing. The ^{10}Be measurements were performed at the ASTER AMS national facility (CEREGE, Aix en Provence) which is supported by the INSU/CNRS, the ANR through the Projets thématiques d'excellence program for the Équipements d'excellence ASTER-CEREGE action and IRD. Pr Fritz Schlunegger and an Anonymous Reviewer are acknowledged for their very constructive comments, which strongly helped to improve the manuscript.

Appendix A. Supplementary data

Supplementary material related to this article can be found, in the online version, at doi:<https://doi.org/10.1016/j.geomorph.2019.106932>.

References

- Ambraseys, N., Bilham, R., 2012. The Sarez-Pamir earthquake and landslide of 18 February 1911. *Seismol. Res. Lett.* 83 (2), 294–314.
- Armijo, R., Lacassin, R., Coudurier-Curvent, A., Carrizo, D., 2015. Coupled tectonic evolution of Andean orogeny and global climate. *Earth Science Reviews* 143, 1–35.
- Arnold, M., Merchel, S., Bourlès, D.L., Braucher, R., Benedetti, L., Finkel, R.C., Aumaître, G., Gottdang, A., Klein, M., 2010. The French accelerator mass spectrometry facil-

- ity ASTER: improved performance and developments. *Nucl. Instrum. Methods Phys. Res. B Beam Interactions with Materials and Atoms* 268, 1954–1959.
- Arnold, M., Aumaître, G., Bourlès, D.L., Keddadouche, K., Braucher, R., Finkel, R.C., Nottoli, E., Benedetti, L., Merchel, S., 2013. The French accelerator mass spectrometry facility ASTER after 4 years: Status and recent developments on ^{36}Cl and ^{129}I . *Nucl. Instrum. Methods Phys. Res. B* 294, 24–28.
- Audin, L., Bechir, A., vol.xxi. 2006. Active Tectonics As Determinant Factor in Landslides Along the Western Cordillera? Congreso Peruano De Geología 13, Extended Abstract of the Sociedad Geologica Del Peru, pp. 237–239.
- Benavente, C., Zerathe, S., Audin, L., Hall, S.R., Robert, X., Delgado, F., Carcaillet, J., Team, A.S.T.E.R., 2017. Active transpressional tectonics in the Andean forearc of southern Peru quantified by ^{10}Be surface exposure dating of an active fault scarp. *Tectonics* 36 (9), 1662–1678.
- Bekaddour, T., Schlunegger, F., Vogel, H., Delunel, R., Norton, K.P., Akçar, N., Kubik, P., 2014. Paleo erosion rates and climate shifts recorded by Quaternary cut-and-fill sequences in the Pisco valley, central Peru. *Earth Planet. Sci. Lett.* 390, 103–115.
- Bissig, T., Riquelme, R., 2010. Andean uplift and climate evolution in the southern Atacama desert deduced from geomorphology and supergene alunite-group minerals. *Earth Planet. Sci. Lett.* 299, 447–457.
- Blodgett, T.A., Isacks, B.L., Lenters, J.D., 1997. Constraints on the origin of paleolake expansions in the central Andes. *Earth Interact.* 1 (1), 1–28.
- Blöthe, J.H., Korup, O., Schwanghart, W., 2015. Large landslides lie low: excess topography in the Himalaya-Karakoram ranges. *Geology* 43 (6), 523–526.
- Borchers, B., Marrero, S., Balco, G., Caffee, M., Goehring, B., Lifton, N., Stone, J., 2016. Geological calibration of spallation production rates in the CRONUS-Earth project. *Quat. Geochronol.* 31, 188–198.
- Braucher, R., Guillou, V., Bourlès, D.L., Arnold, M., Aumaître, G., Keddadouche, K., Nottoli, E., 2015. Preparation of ASTER in-house $^{10}\text{Be}/^{9}\text{Be}$ standard solutions. *Nucl. Instrum. Methods Phys. Res. B Beam Interactions with Materials and Atoms* 361, 335–340.
- Broxton, M.J., Edwards, L.J., 2008. Lunar and Planetary Science Conference The Ames stereo pipeline: automated 3D surface reconstruction from orbital imagery, vol 39, abstract 2419.
- Casagli, N., Ermini, L., 1999. Geomorphic analysis of landslide dams in the northern Apennine. *Transaction of the Japanese Geomorphologic Union* 20, 219–249.
- Chiou, B.S.J., Youngs, R.R., 2014. Update of the Chiou and Youngs NGA model for the average horizontal component of peak ground motion and response spectra. *Earthq. Spectra* 30 (3), 1117–1153.
- Crosta, G.B., Hermanns, R.L., Dehls, J., Lari, S., Sepulveda, S., 2017. Rock avalanches clusters along the northern Chile coastal scarp. *Geomorphology* 289, 27–43.
- Crosta, G.B., Hermanns, R.L., Frattini, P., Valbusi, E., Valagussa, A., 2014. Large slope instabilities in Northern Chile: inventory, characterisation and possible triggers. In: Proceedings of the 3rd World Landslide Forum, 2–6 June 2014, Beijing, http://dx.doi.org/10.1007/978-3-319-04996-0_28, p 6.
- Delgado, F., Zerathe, S., Audin, I., Robert, X., Litty, C., Benavente, C., Carcaillet, J., Team, A., 2018. Quantifying basin-average denudation rates over the past 20 ka from landslide-dammed lake sediments in the South Western Peruvian Andes. EGU General Assembly Conference Abstracts (Vol. 20, P. 16124).
- Duman, T.Y., 2009. The largest landslide dam in Turkey: tortum landslide. *Eng. Geol.* 104 (1–2), 66–79.
- Dunai, T.J., Gonzalez López, G.A., Juez-Larré, J., 2005. Oligocene–Miocene age of aridity in the Atacama desert revealed by exposure dating of erosion-sensitive landforms. *Geology* 33 (4), 321–324.
- Evenstar, L., Stuart, F.M., Hartley, A.J., Tattitch, B., 2015. Slow Cenozoic uplift of the western Andean Cordillera indicated by cosmogenic ^{3}He in alluvial boulders from the Pacific Planation Surface. *Geophys. Res. Lett.* 82, 8448–9455.
- Ehlers, T.A., Poulsen, C.J., 2009. Influence of Andean uplift on climate and paleoaltimetry estimates. *Earth Planet. Sci. Lett.* 281, 238–248.
- García, M., Riquelme, R., Farías, M., Hérail, G., Charrier, R., 2011. Late Miocene-holocene canyon incision in the western Altiplano, northern Chile: tectonic or climatic forcing? *J. Geol. Soc.* 168, 1047–1060.
- Glade, T., Crozier, M.J., 2005. The nature of landslide hazard impact. In: *Landslide Hazard and Risk*, pp. 43–74.
- Gorum, T., Fan, X., van Westen, C.J., Huang, R.Q., Xu, Q., Tang, C., Wang, G., 2011. Distribution pattern of earthquake-induced landslides triggered by the 12 May 2008 Wenchuan earthquake. *Geomorphology* 133 (3–4), 152–167.
- Gosse, J.C., Phillips, F.M., 2001. Terrestrial in situ cosmogenic nuclides: theory and application. *Quat. Sci. Rev.* 20 (14), 1475–1560, [http://dx.doi.org/10.1016/S0277-3791\(00\)00171-2](http://dx.doi.org/10.1016/S0277-3791(00)00171-2).
- Gunnell, Y., Thouret, J.C., Brichau, S., Carter, A., Gallagher, K., 2010. Low-temperature thermochronology in the Peruvian Central Andes: implications for long-term continental denudation, timing of plateau uplift, canyon incision and lithosphere dynamics. *J. Geol. Soc.* 167 (4), 803–815.
- Hall, S.R., Farber, D.L., Audin, L., Finkel, R.C., 2012. Recently active contractile deformation in the forearc of southern Peru. *Earth Planet. Sci. Lett.* 337, 85–92.
- Hermanns, R.L., Niedermann, S., Villanueva Garcia, A., Sosa Gomez, J., Strecker, M.R., 2001. Neotectonics and catastrophic failure of mountain fronts in the southern intra-Andean Puna plateau, Argentina. *Geology* 29 (7), 619–623.
- Hermanns, R., Niedermann, S., Kubik, P., 2004. Rock avalanching into a landslidedammed lake causing multiple dam failure in Las Conchas valley (NW Argentina) – evidence from surface exposure dating and stratigraphic analyses. *Landslides* 1, 113–122.
- Hermanns, R., Niedermann, S., Villanueva Garcia, A., Schellenberger, A., 2006. Rock avalanching in the NW Argentine Andes as a result of complex interactions of lithologic, structural and topographic boundary conditions, climate change and active tectonics: landslides from massive rock slope failure. *NATO Science Series IV* 49, 539–569.
- Hermanns, R.L., Schellenberger, A., 2008. Quaternary tephrochronology helps define conditioning factors and triggering mechanisms of rock avalanches in NW Argentina. *Quat. Int.* 178 (1), 261–275.
- Hermanns, R.L., Hewitt, K., Strom, A., Evans, S.G., Dunning, S.A., Scarascia-Mugnozza, G., 2011. The classification of rockslide dams. In: *Natural and Artificial Rockslide Dams*. Springer, Berlin, Heidelberg, pp. 581–593.
- Houston, J., Hartley, A.J., 2003. The central Andean west-slope rainshadow and its potential contribution to the origin of hyper-aridity in the Atacama desert. *Int. J. Climatol.* 23 (12), 1453–1464.
- Huffman, G.J., Bolvin, D.T., Nelkin, E.J., Wolff, D.B., Adler, R.F., Gu, G., Stocker, E.F., 2007. The TRMM multisatellite precipitation analysis (TMPA): quasi-global, multiyear, combined-sensor precipitation estimates at fine scales. *J. Hydrometeorol.* 8 (1), 38–55.
- Humair, F., Pedrazzini, A., Epard, J.-L., Froese, C.R., Jaboyedoff, M., 2013. Structural characterization of Turtle Mountain anticline (Alberta, Canada) and impact on rock slope failure. *Tectonophysics* 605, 133–148.
- Insel, N., Poulsen, C.J., Ehlers, T.A., Sturm, C., 2012. Response of meteoric $\delta^{18}\text{O}$ to surface uplift—Implications for Cenozoic Andean Plateau growth. *Earth and Planetary Science Letters* *Earth Planet. Sci. Lett.* 317, 262–272.
- Jeffery, M.J., Ehlers, T.A., Yanites, B.J., Poulsen, C.J., 2013. Quantifying the role of paleoclimate and Andean Plateau uplift on river incision. *J. Geophys. Res. Earth Surf.* 118, 852–871.
- Keefer, D.K., Moseley, M.E., deFrance, S.D., 2003. A 38,000-year record of floods and debris flows in the ilo region of southern peru and its relation to el niño events and great earthquakes. *Palaeogeogr. Palaeoclimatol. Palaeoecol.* 194, 41–77.
- Korup, O., 2004. Geomorphometric characteristics of New Zealand landslide dams. *Eng. Geol.* 73 (1–2), 13–35.
- Korup, O., Clague, J.J., Hermanns, R.L., Hewitt, K., Strom, A.L., Weidinger, J.T., 2007. Giant landslides, topography, and erosion. *Earth Planet. Sci. Lett.* 261 (3–4), 578–589.
- Lifton, N., Sato, T., Dunai, T.J., 2014. Scaling in situ cosmogenic nuclide production rates using analytical approximations to atmospheric cosmic-ray fluxes. *Earth Planet. Sci. Lett.* 386, 149–160, <http://dx.doi.org/10.1016/j.epsl.2013.10.052>.
- Litty, C., Lanari, P., Burn, M., Schlunegger, F., 2017. Climate-controlled shifts in sediment provenance inferred from detrital zircon ages, western Peruvian Andes. *Geology* 45 (1), 59–62.
- Madella, A., Delunel, R., Akçar, N., Schlunegger, F., Christl, M., 2018. ^{10}Be -inferred paleo-denudation rates imply that the mid-Miocene western central Andes eroded as slowly as today. *Sci. Rep.* 8 (1), 2299.
- Margirier, A., Audin, L., Carcaillet, J., Schwartz, S., 2015. Tectonic and climatic controls on the Chuquibamba landslide (western Andes, southern Peru). *Earth Surf. Dyn. Discuss.* 2, 1129–1153.
- Marrero, S.M., Phillips, F.M., Borchers, B., Lifton, N., Aumer, R., Balco, G., 2016. Cosmogenic nuclide systematics and the CRONUScalc program. *Quat. Geochronol.* 31, 160–187, <http://dx.doi.org/10.1016/j.quageo.2015.09.005>.
- Martin, L.C., Blard, P.H., Lavé, J., Condom, T., Prémaillon, M., Jomelli, V., Tibari, B., 2018. Lake Tauca highstand (Heinrich Stadial 1a) driven by a southward shift of the Bolivian High. *Sci. Adv.* 4 (8), eaar2514.
- Mather, A.E., Hartley, A.J., Griffiths, J.S., 2014. The giant coastal landslides of Northern Chile: tectonic and climate interactions on a classic convergent plate margin. *Earth Planet. Sci. Lett.* 388, 249–256.
- McPhillips, D., Bierman, P.R., Rood, D.H., 2014. Millennial-scale record of landslides in the Andes consistent with earthquake trigger. *Nat. Geosci.* 7, 925–930.
- Moreiras, S.M., Sepúlveda, S.A., 2015. Megalandslides in the Andes of central Chile and Argentina (32° – 34° S) and potential hazards. *Geol. Soc. London Spec. Publ.* 399 (1), 329–344.
- Moreiras, S.M., Hermanns, R.L., Fauqué, L., 2015. Cosmogenic dating of rock avalanches constraining Quaternary stratigraphy and regional neotectonics in the Argentine Central Andes (32° S). *Quat. Sci. Rev.* 112, 45–58.
- Nicoletti, P.G., Parise, M., 2002. Seven landslide dams of old seismic origin in southeastern Sicily (Italy). *Geomorphology* 46 (3–4), 203–222.
- Nishiizumi, K., Caffee, M.W., Finkel, R.C., Brimhall, G., Mote, T., 2005. Remnants of a fossil alluvial fan landscape of Miocene age in the Atacama desert of northern Chile using cosmogenic nuclide exposure age dating. *Earth Planet. Sci. Lett.* 237, 499–507.
- Pinto, L., Hérail, G., Sepúlveda, S.A., Krop, P., 2008. A Neogene giant landslide in Tarapacá, northern Chile: a signal of instability of the westernmost Altiplano and palaeoseismicity effects. *Geomorphology* 102 (3–4), 532–541.
- Placzek, C., Quade, J., Betancourt, J.L., 2001. Holocene lake-level fluctuations of Lake Aricota, southern Peru. *Quat. Res.* 56 (2), 181–190.
- Placzek, C.J., Quade, J., Patchett, P.J., 2013. A 130 ka reconstruction of rainfall on the Bolivian Altiplano. *Earth Planet. Sci. Lett.* 363, 97–108.
- Rech, J.A., Currie, B.S., Jordan, T.E., Riquelme, R., Lehmann, S.B., Kirk-Lawlor, N.E., Li, S., Gooley, J.T., 2019. Massive middle Miocene gypsiferous paleosols in the Atacama desert and the formation of the Central Andean rain-shadow. *Earth Planet. Sci. Lett.* 506, 184–194.
- Schildgen, T.F., Ehlers, T.A., Whipple, K.X., Whipp, D.M., van Soest, M.C., Hodges, K.V., 2009. Quantifying canyon incision and Andean Plateau surface uplift, southwest Peru: a thermochronometer and numerical modeling approach. *J. Geophys. Res. Earth Surf.* 114, FO4014.
- Schlunegger, F., Zeilinger, G., Kounov, A., Kober, F., Hüser, B., 2006. Scale of relief growth in the forearc of the Andes of Northern Chile (Arica latitude, 18° S). *Terra Nova* 18, 217–223.

- Sempere, T., Folguera, A., Gerbault, M., 2008. *Tectonophysics New Insights into the Andean Evolution: an Introduction to Contributions from the 6th IASAG Symposium* (Barcelona, 2005), vol. 459, pp. 1–13.
- Shreve, R.L., 1968. The blackhawk landslide: geological society of america. Special Paper 108, 4–47.
- Steffen, D., Schlunegger, F., Preusser, F., 2010. Late Pleistocene fans and terraces in the Majes valley, southern Peru, and their relation to climatic variations. *Int. J. Earth Sci.* 99 (8), 1975–1989.
- Strom, A.L., 2006. Morphology and internal structure of rockslides and rock avalanches: grounds and constraints for their modelling. In: Evans, S.G., Scarascia Mugnozza, G., Strom, A.L., Hermanns, R.L. (Eds.), *Landslides from Massive Rock Slope Failures 49*. Dordrecht. Springer.
- Strasser, M., Schlunegger, F., 2005. Erosional processes, topographic length-scales and geomorphic evolution in arid climatic environments: the 'Lluta collapse', northern Chile. *Int. J. Earth Sci.* 94 (3), 433–446.
- Thouret, J.C., Gunnell, Y., Jicha, B.R., Paquette, J.L., Braucher, R., 2017. Canyon incision chronology based on ignimbrite stratigraphy and cut-and-fill sediment sequences in SW Peru documents intermittent uplift of the western Central Andes. *Geomorphology* 298, 1–19.
- Thouret, J.C., Wörner, G., Gunnell, Y., Singer, B., Zhang, X., Souriot, T., 2007. Geochronologic and stratigraphic constraints on canyon incision and Miocene uplift of the Central Andes in Peru. *Earth Planet. Sci. Lett.* 263 (3–4), 151–166.
- Trauth, M.H., Bookhagen, B., Marwan, N., Strecker, M.R., 2003. Multiple landslide clusters record Quaternary climate changes in the northwestern Argentine Andes. *Palaeogeogr. Palaeoclimatol. Palaeoecol.* 194 (1–3), 109–121.
- Villegas-Lanza, J.C., Chlieh, M., Cavalié, O., Tavera, H., Baby, P., Chire-Chira, J., Nochet, J.-M., 2016. Active tectonics of Peru: Heterogeneous interseismic coupling along the Nazca megathrust, rigid motion of the Peruvian Sliver, and Subandean shortening accommodation. *J. Geophys. Res. Solid Earth* 121, 7371–7394, <http://dx.doi.org/10.1002/2016JB013080>.
- Viveen, W., Schlunegger, F., 2018. Prolonged extension and subsidence of the Peruvian forearc during the Cenozoic. *Tectonophysics* 730, 48–62.
- Wayne, W.J., 1999. The Alemania rockfall dam: a record of a mid-holocene earthquake and catastrophic flood in northwestern Argentina. *Geomorphology* 27 (3–4), 295–306.
- Wörner, G., Uhlig, D., Kohler, I., Seyfried, H., 2002. Evolution of the West Andean Escarpment at 18°S (N. Chile) during the last 25 Ma: uplift, erosion and collapse through time. *Tectonophysics* 345 (1–4), 183–198.
- Zerathe, S., Blard, P.H., Braucher, R., Bourlès, D., Audin, L., Carcaillet, J., Delgado, F., Benavente, C., Keddadouche, K., 2017. Toward the feldspar alternative for cosmogenic ^{10}Be applications. *Quat. Geochronol.* 41, 83–96.